ALLOYS FOR ADVANCED STEAM TURBINES—OXIDATION BEHAVIOR

G. R. Holcomb
National Energy Technology Laboratory
U. S. Department of Energy
1450 Queen Avenue SW
Albany, Oregon 97321

Abstract

Advanced or ultra supercritical (USC) steam power plants offer the promise of higher efficiencies and lower emissions. Current goals of the U.S. Department of Energy (DOE) include power generation from coal at 60% efficiency, which would require steam temperatures of up to 760°C. Current research on the oxidation of candidate materials for advanced steam turbines is presented with a focus on a methodology for estimating chromium evaporation rates from protective chromia scales. The high velocities and pressures of advanced steam turbines lead to evaporation predictions as high as 5×10^{-8} kg $m^{-2}s^{-1}$ of $CrO_2(OH)_2(g)$ at 760°C and 34.5 MPa. This is equivalent to 0.077 mm per year of solid Cr loss.

Introduction

Current goals of the U.S. Department of Energy's Advanced Power Systems Initiatives include power generation from coal at 60% efficiency, which would require steam conditions of up to 760°C and 35MPa, so called ultra-supercritical (USC) steam conditions. This is in comparison to conventional sub-critical steam plants which operate at about 37% efficiency (steam at 540°C-14.5 MPa) and advanced plants that are currently just being introduced into the market that operate at 40 to 45% efficiency (steam at 600°C-28MPa). The importance of increased efficiency is because it is estimated that for each 1% raise in plant efficiency will eliminate approximately 1,000,000 tons of CO_2 over the lifetime of an 800MW coal fired plant (1). The overarching limitation to achieving the DOE goal is a lack of cost effective metallic materials that can perform at these temperatures and pressures (2). Improving alloy resistance to high temperature corrosion is one key in developing new, efficient and clean coal-fired ultra-supercritical (USC) steam plants (2).

For the USC application, both turbine and boiler materials will operate at higher temperatures and pressures than in conventional plants. However, the development of

creep strength in alloys is often obtained at the expense of corrosion and oxidation resistance. Therefore, the strategies to confer corrosion resistance may be needed if ever increasing cycle temperatures are to be achieved in advanced plants. To identify or develop alloys and strategies that can meet these performance requirements, it is critical to understand the degradation mechanisms that will occur during operation.

A critical aspect of materials usage in USC steam turbines is oxidation behavior. Oxidation can result in several adverse conditions: general section loss from material thinning, deep and localized section loss from internal oxidation along grain boundaries, dimensional changes that are critical in airfoils, and downstream erosion from oxide spallation. Evaporation of protective chromia scales may also be an issue at the higher temperatures and pressures of USC steam turbines. The evaporation of chromia scales is the focus of the research presented here.

Chromia Evaporation

The oxidation of alloys protected by the formation of Cr_2O_3 (chromia formers) can undergo scale loss due to reactive evaporation of chromium containing gas species. Water vapor increases the evaporation loss by allowing the formation of $CrO_2(OH)_2(g)$, which for the same conditions has a higher vapor pressure than $CrO_3(g)$. $CrO_3(g)$ is the primary Cr gas specie in dry air or oxygen. A generalized reaction equation for Cr evaporation from Cr_2O_3 is

$$\tfrac{1}{2}Cr_2O_3(s) + nH_2O(g) + mO_2(g) = CrO_{1.5+n+2m}H_{2n}(g) \quad (1)$$

For $CrO_2(OH)_2(g)$, n=1 and m= ¾ so Eq. 1 becomes:

$$\tfrac{1}{2}Cr_2O_3(s) + H_2O(g) + \tfrac{3}{4}O_2(g) = CrO_2(OH)_2(g) \quad (2)$$

Evaporation can change the overall oxidation kinetics from parabolic behavior to linear kinetics or even to breakaway oxidation. Linear kinetics can arise after scale growth from oxidation, which decreases with increasing scale thickness, matches the scale loss from reactive evaporation. The change in scale thickness, x, with time, t, can be described in terms of the parabolic rate constant, k_p, and the linear reactive evaporation rate, k_e, as:

$$\frac{dx}{dt} = \frac{k_p}{x} - k_e \quad (3)$$

At long times or high reactive evaporation rates, a limiting scale thickness, x_L, arises that is given by:

$$x_L = \frac{k_p}{k_e} \quad (4)$$

In this case metal loss rates are linear, but still involve diffusion through a protective scale. Rapid metal loss can occur when reactive evaporation of Cr depletes the scale (and sometimes the substrate metal) of Cr (3-4). Decreased Cr in the scale or metal can lead to the formation of less protective oxides, such as Fe-Cr oxides in Fe-Cr base alloys. Unprotective scales can lead to rapid metal loss, or "break-away" oxidation.

A methodology for calculating evaporation rates in a high pressure steam turbine is presented. Experimental results were used to validate the methodology.

Methodology

Evaporation

One way to determine evaporation rates is to assume that volatility is limited by the transport of the volatile specie through a boundary layer in the gas phase. For flat plate geometry with laminar flow, the evaporation rate can be calculated by Eq. 5 (5-6):

$$k_e\left(\frac{kg}{m^2 s}\right) = 0.664\, Re^{0.5} Sc^{0.343} \frac{D_{AB}\rho}{L} \tag{5}$$

Where Re and Sc are the dimensionless Reynolds and Schmidt numbers, D_{AB} is the gaseous diffusion coefficient between the Cr gas specie and the solvent gas ($m^2 s^{-1}$), ρ is the density (kg m^{-3}) of the evaporative specie in the gas, and L is the length (m) in the flow direction of the flat plate. Equation 5 is valid for Sc numbers between 0.6 and 50 (5). Assuming ideal gas behavior and a reaction described by Eq. 1, this can be expanded to:

$$k_e\left(\frac{kg}{m^2 s}\right) = 0.664\, Re^{0.5} Sc^{0.343} \frac{D_{AB} M_i P_T}{LRT} P_{H_2O}^n P_{O_2}^m \exp\left(-\frac{\Delta G}{RT}\right) \tag{6}$$

Where P_T is the total pressure (Pa), P_i is the partial pressure of gas specie i, M_i is the molecular mass (kg mol^{-1}) of gas specie i (in this case i is the Cr-containing gas specie), and ΔG is the Gibbs energy of Eq. 1 (J mol^{-1}). The dimensionless Reynolds and Schmidt numbers are defined as:

$$Re = \frac{\rho_s v L}{\eta} \tag{7}$$

$$Sc = \frac{\eta}{\rho_s D_{AB}} \tag{8}$$

Where ρ_s is the density of the solvent gas (kg m^{-3}), η is the absolute viscosity (kg $m^{-1} s^{-1}$) and v is the gas velocity (m s^{-1}).

For turbulent flow ($Re > 5\times10^5$), the equation equivalent to Eq. 6 is (5):

$$k_e\left(\frac{kg}{m^2 s}\right) = 0.0592\, Re^{4/5} Sc^{1/3} \frac{D_{AB} M_i P_T}{LRT} P_{H_2O}^n P_{O_2}^m \exp\left(-\frac{\Delta G}{RT}\right) \quad (9)$$

Each of the parameters in Eqs. (6-9) that require additional commentary are described.

Diffusion Coefficient, D_{AB}

Estimation of the diffusion coefficient, D_{AB}, between the Cr gas species and the solvent gas is the most tenuous of the parameters. Tucker and Nelken (7) compared several different methods for estimation of D_{AB} and of two recommended choices, the one developed by Fuller *et al.* (8) was used here because it contains fewer parameters that themselves need to be estimated. After conversion to SI units, the estimation equation is:

$$D_{AB} = \frac{(3.203\times10^{-4})T^{1.75}}{P_T(v_A^{1/3} + v_B^{1/3})^2}\sqrt{\frac{1}{M_A}+\frac{1}{M_B}} \quad (10)$$

Here v_i is the diffusion volume of species i ($m^3\ mol^{-1}$). Diffusion volumes, as given by Fuller *et al.* (8), were from a fit of Eq. 10 with an extensive list of diffusion data measurements of various A-B pairs. Diffusion volumes of Cr gas species are not available and so were estimated based on a molecule with a radius of 1.6×10^{-10} m, then converted to molar volume. The value of 1.6×10^{-10} m comes from a density functional theory estimation of the length of a Cr-O bond in CrO (9). The values of v_i for the mixtures other than air were based on a weighted average of the component v_i values.

An additional consideration for supercritical steam turbine environments is that D_{AB} can diverge from the inverse pressure relationship of Eq. 10 at high pressures (10). The method in Bird *et al.* (10) was used to approximate this divergence using reduced temperature and pressure, T_r and P_r. Reduced temperature and pressure are equal to $T/T_{critical}$ and $P/P_{critical}$. For water $T_{critical}$ is 647.25 K and $P_{critical}$ is 218.25 MPa. As an example, consider the conditions of 760°C and 34.5 MPa. In this case T_r is 1.60 and P_r is 1.56, which from Bird (10) reduces the value of D_{AB} obtained from Eq. 10 by a factor of 0.88. This is an approximation because this method was developed for self-diffusivity using Enskog kinetic theory and fragmentary data (11).

Absolute Viscosity, η

The absolute viscosity of non-polar gases, for example O_2, N_2, Ar, and air, can be calculated from the following equation (7-8):

$$\eta = 8.44\times10^{-25}\frac{\sqrt{MT}}{\sigma^2\Omega_\eta} \quad (11)$$

Where σ is a characteristic diameter of the molecule (m) and Ω_η is the dimensionless collision integral. Literature values of σ and Ω_η were used (5-6).

The absolute viscosity of water, in the temperature range of interest, can be found using Eq. 12, which was obtained from linear portions of absolute viscosity curves as functions of temperature and pressure (12). Equation 12 is for the temperature range 811K-1089K and pressures up to 3.45×10^7 Pa where the linear fit has a correlation coefficient (R^2) of 0.994. Absolute viscosity for temperatures below 811K, nearer to the critical point of water, are decidedly non-linear and Eq. 12 should not be used.

$$\eta = 3.701\times10^{-8} + 3.080\times10^{-7}T + 1.144\times10^{-13}P_T \tag{12}$$

For gas mixtures, the absolute viscosity of each component gas was combined using Eqs. 13-14 (5-6):

$$\eta_{mix} = \sum_{i=1}^{n} \frac{x_i\eta_i}{\sum_{j=1}^{n} x_j\Phi_{ij}} \tag{13}$$

$$\Phi_{ij} = \frac{1}{\sqrt{8}}\left(1+\frac{M_i}{M_j}\right)^{-1/2}\left[1+\left(\frac{\eta_i}{\eta_j}\right)^{1/2}\left(\frac{M_j}{M_i}\right)^{1/4}\right]^2 \tag{14}$$

Solvent Gas Density, ρ_s

The density of the solvent gas is found by assuming ideal gas behavior, which allows Eq. 15:

$$\rho_s = \frac{P_T M_{Ave}}{RT} \tag{15}$$

where M_{Ave} is the average molecular weight of the solvent gas mixture.

Gibbs Energy, ΔG

The two primary Cr gas species for reactive evaporation are CrO_3(g) in either dry conditions or moist conditions at higher temperatures, and $CrO_2(OH)_2$(g) in moist conditions at most of the temperatures of interest here. Equation 1 describes the evaporation reaction. It is necessary to know the Gibbs energy of formation for each of the products and reactants in Eq. 1 to obtain the ΔG of the reaction used in Eqs. 6 and 9. The ΔG of Eq. 1 is given by:

$$\Delta G_1 = -RT\ln\frac{P_{CrO_{1.5+n+2m}H_{2n}}}{a_{Cr_2O_3}^{1/2}P_{O_2}^{m}P_{H_2O}^{n}} \tag{16}$$

The ΔG_f for $CrO_2(OH)_2(g)$ is not well established. Opila (13) has reviewed the literature and has found that using data based on Glusko (14) results in much lower calculated partial pressures of $CrO_2(OH)_2(g)$ than using data based on Ebbinghaus (15). Glusko (14) is the source of $CrO_2(OH)_2(g)$ data for the ITVAN (16) and HSC (17) thermodynamics programs. The experimental data of Gindorf *et al.* (18) lie between that predicted by Glusko (14) and Ebbinghaus (15) (in terms of log $P_{CrO2(OH)2}$). Ebbinghaus (15) used estimates of molecular parameters to formulate thermodynamic information. Gindorf *et al.* (18) used transpiration experiments to measure the partial pressure of $CrO_2(OH)_2(g)$. It is unclear (13) how the Glusko (14) data was generated. Table 1 shows ΔG_f values for compounds and species of interest.

Table 1 – Gibbs Energy of Formation for Species of Interest. Calculated from Roine (17) Unless Otherwise Indicated.

T (K)	ΔG_f $Cr_2O^3(s)$ (J mol^{-1})	ΔG_f $H_2O(g)$ (J mol^{-1})	ΔG_f CrO_3 (J mol^{-1})	ΔG_f $CrO_2(OH)_2$ (J mol^{-1}) (Glusko 14)	ΔG_f $CrO_2(OH)_2$ (J mol^{-1}) (Gindorf 18)	ΔG_f $CrO_2(OH)_2$ (J mol^{-1}) (Ebbinghaus 15)
500	-998,700	-219,100	-292,200	-616,600	-632,100	-644,700
573	-979,300	-215,400	-287,400	-599,000	-615,100	-629,500
600	-972,300	-214,000	-285,700	-592,500	-608,900	-624,000
673	-954,300	-210,300	-280,900	-574,900	-592,500	-608,900
700	-947,400	-208,900	-279,200	-568,400	-586,300	-603,400
773	-928,700	-205,000	-274,400	-550,900	-569,400	-588,300
800	-921,800	-203,600	-272,600	-544,400	-563,300	-582,800
873	-903,300	-199,700	-267,800	-526,900	-546,400	-567,700
900	-896,500	-198,200	-266,100	-520,500	-540,200	-562,200
973	-878,100	-194,200	-261,200	-503,000	-523,400	-547,200
1000	-871,300	-192,700	-259,500	-496,500	-517,200	-541,700

The partial pressures of $CrO_3(g)$ and $CrO_2(OH)_2(g)$ over pure Cr_2O_3 (activity of 1) were found for conditions of atmospheric pressure, $P_{O2} = 0.20$, and $P_{H2O} = 0.03$ (air plus 3%

H_2O) and are shown in Fig. 1a. Figures 1b and 1c also show partial pressures of CrO_3(g) and $CrO_2(OH)_2$(g) over pure Cr_2O_3, but in these cases for H_2O with 180 ppb dissolved O_2 (DO). Figure 1b is at atmospheric pressure and Fig. 1c is at 30.0 MPa.

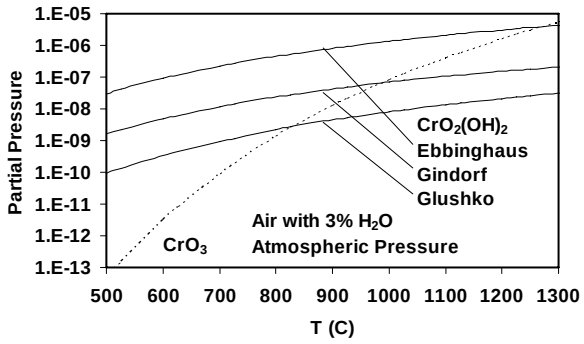

a)

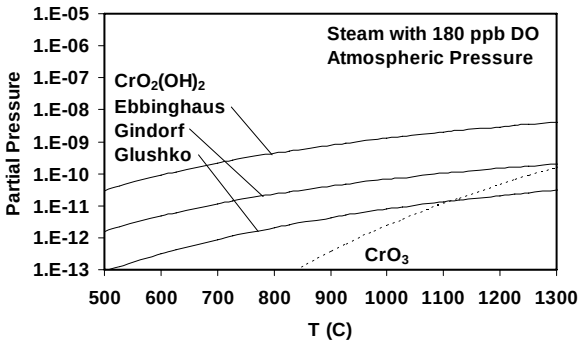

b)

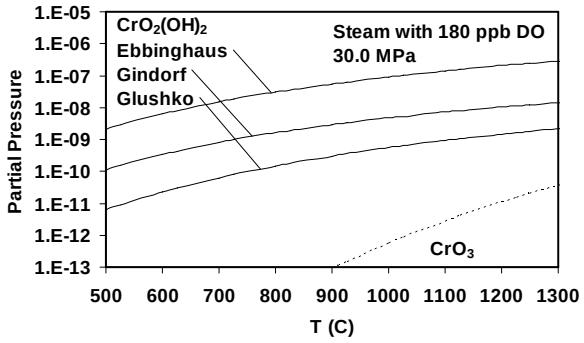

c)

Figure 1. Partial pressures of CrO_3(g) and $CrO_2(OH)_2$(g) over pure Cr_2O_3 (activity of 1) for a) 3% H_2O in air at atmospheric pressure, b) steam with 180 ppb DO at atmospheric pressure, and c) steam with 180 ppb DO at 30.0 MPa.

Gibbs energies for partial pressures above atmospheric were calculated by adjusting ΔG_f of each compound or specie using:

$$\Delta G_{f,P} = \Delta G_f^\circ + \left(n_{gas\ prod} - n_{gas\ react}\right) RT \ln \frac{P_T}{P_T^\circ} \qquad (17)$$

Equation 17 assumes that all changes in ΔG_f due to pressure are from the gas phase and follow ideal gas behavior. In Eq. 17, ($n_{gas\ prod}$ – $n_{gas\ react}$) is the change in the number of moles of gas to form the compound or specie. P_T° and ΔG_f° are P_T and ΔG_f at atmospheric pressure.

Since the formation of $CrO_2(OH)_2$(g) reduces the total moles of gas, higher pressures increase its partial pressure (Figs. 1b-1c). Conversely the formation of CrO_3(g) increases the total moles of gas, so higher pressures decrease its partial pressure (Figs. 1b-1c).

Experimental Comparison

Experiments best suited to verify the methodology have situations where a steady-state scale thickness (Eq. 4) is quickly established and mass loss due to reactive evaporation of Cr_2O_3 can be found from mass change with time measurements. Several such tests are described below. Otherwise it would be necessary to separate the effects from scale growth from oxidation and scale thinning from evaporation by the integration of Eq. 3, from which it can be difficult to obtain reliable k_p and k_e values.

Cyclic oxidation experiments on Haynes 230 (UNS NO6230) (19) and Inconel 625 (UNS NO6625) were conducted in air in the presence of steam at atmospheric pressure. The compositions of these alloys are given in Table 2. This was designed to examine the adhesion and spallation behavior of protective oxides. The tests consisted of 1-hour cycles of heating and cooling (55 minutes in the furnace and 5 minutes out of the furnace) in a tube furnace equipped with a programmable slide to raise and lower the samples, Fig. 2. Periodically (between cycles) the samples were removed for mass measurements and then returned for more exposure. The suspension of the samples as shown in Fig. 2 allowed the passage of the gas steam to flow unimpeded across the samples. Water was metered into the bottom of the furnace along with compressed air. Two total gas flow rates were used with rates of 1.9×10^{-3} m s^{-1} (38% water vapor and air, by volume) and 7.6×10^{-3} m s^{-1} (37% water vapor and air, by volume). The exposure temperature for these tests was 760°C. There was no evidence of scale spallation during these tests. In similar tests on certain other alloys, for example with TP347HFG, there was evidence of scale spallation from visible scale debris from handling during mass measurements.

Table 2 – Alloy Compositions as Found by X-ray Florescence (XRF) for the Nickel Alloys or the Nominal Composition for 304L Stainless Steel.

Alloy	Type	Fe	Cr	Ni	Mo	Nb	Mn	Si	Cu	Al	Other
Haynes 230	XRF	1.3	22.6	58.8	1.3		0.5	0.3	0.04	0.4	14.3 W
Inconel 625	XRF	4.4	21.4	61.0	8.4	3.4	0.1	0.4	0.3	0.2	0.3 Ti 0.01 V 0.07 Co
304L	Nom	Bal	19.0	10.0							

Note that the reactive evaporation rates calculated from the preceding methodology are on a $CrO_2(OH)_2(g)$ basis and the experimental mass losses were from chromia scale

evaporation and so are on a Cr_2O_3(s) basis. To compare the two rates on the same Cr_2O_3 basis, the following conversion was used:

$$k_e[Cr_2O_3\ basis] = \frac{M_{Cr2O3}}{2M_{CrO2(OH)2}} k_e[CrO_2(OH)_2\ basis] = 0.644 k_e[CrO_2(OH)_2\ basis] \quad (18)$$

Figure 2. Cyclic oxidation apparatus for testing in atmospheric pressure steam/air mixtures.

Results from these tests are shown in Fig. 3 in comparison with predicted slopes from reactive evaporation of Cr_2O_3(s) to $CrO_2(OH)_2$(g) using the Gindorf *et al.* (18) data for $CrO_2(OH)_2$(g). The agreement is close, suggesting that the reactive evaporation methodology is validated for this case.

Figure 4 is a backscattered electron micrograph of Haynes 230 (UNS NO6230) after exposure at 760°C in moist air for 2000 cycles. It shows a very thin oxide scale, approximately 1 μm thick. Aluminum was internally oxidized.

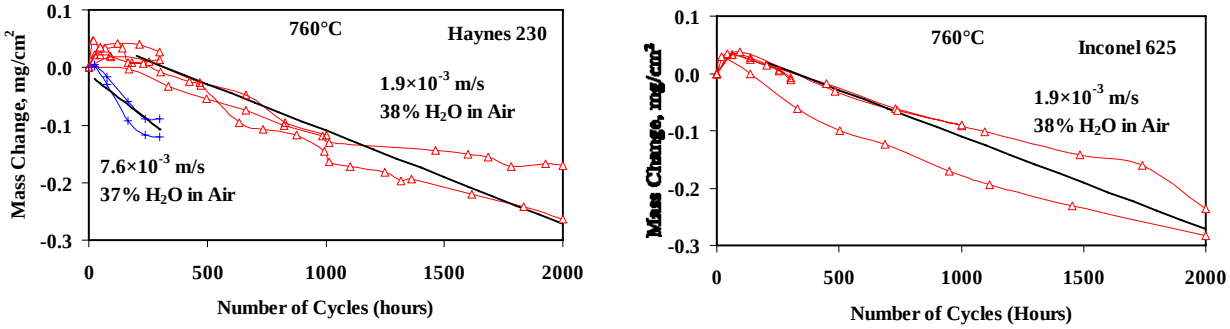

Figure 3. Cyclic oxidation of Haynes 230 (UNS NO6230) (19) and Inconel 625 (UNS NO6625) at 760°C in moist air. Triangle data points for 1.9×10^{-3} m s^{-1} and plus data points for 7.6×10^{-4} m s^{-1}. Straight solid lines are the predicted slopes (on a Cr_2O_3 basis) from reactive evaporation of Cr_2O_3(s) to $CrO_2(OH)_2$(g) using the Gindorf *et al.* (18) data for $CrO_2(OH)_2$(g).

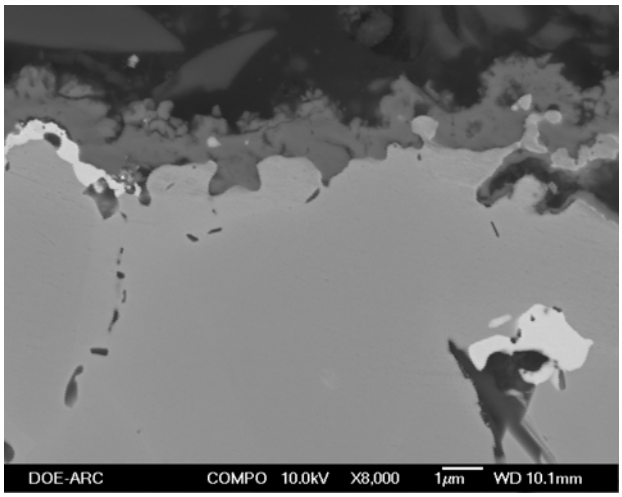

Figure 4. Micrograph using backscattered electrons of Haynes 230 (UNS NO6230) after exposure at 760°C in moist air for 2000 cycles (19). The scale is predominately Cr_2O_3. The bright second phase is W-rich.

Table 3 shows a comparison of the experimental slopes (after 200 hours for the 1.9×10^{-3} m s^{-1} data and after 24 hours with the 7.7×10^{-3} m s^{-1} data) and the predicted reactive evaporation rates using the three sets of ΔG_f data for $CrO_2(OH)_2(g)$. The evaporation model results using Gindorf ΔG values are in good to excellent agreement with experimental values.

Table 3 also compares experimental results from Asteman *et al.* (5) for 304L (UNS S30403, composition in Table 2) at 600°C in 10% H_2O in O_2. In this case evaporation was evident from 72 to 168 hours of exposure. Once again there is good agreement between experiment and evaporation rates calculated using the Gindorf *et al.* (18) data for $CrO_2(OH)_2(g)$.

For the applications and experimental design discussions that follow, the Gindorf *et al.* (18) data for $CrO_2(OH)_2(g)$ is used.

Asteman *et al.* (4) also showed breakaway oxidation for 304L at 600°C in 40% H_2O in O_2. For a gas mixture of H_2O and O_2, the equilibrium constant in Eq. 2 can be used to show that the partial pressure of $CrO_2(OH)_2(g)$ is at a maximum with $P_{H2O} = 4/7P_{O2}$ (~57% H_2O). So increasing the water content in Asteman *et al.* (4) from 10% to 40% increased the evaporation rate, which led to breakaway oxidation due to a depletion of Cr in the scale.

Supercritical Steam Turbine Environments

Development of advanced steam turbines is underway in much of the world to improve the efficiency of power generation from coal. While much of the alloy development involves improving high temperature creep strength, steam oxidation resistance is also of importance. Current U.S. DOE research programs are aimed at 60% efficiency from coal generation, which would require increasing the operating conditions to as high as 760°C and 37.9 MPa for the high pressure (HP) turbine. Current technology limits operation to about 620°C. Above 650°C, it is expected that nickel-base alloys will be required based on creep strength limitations of ferritic and austenitic stainless steels.

Table 3 – Comparison of Experimental and Predicted Evaporation Rates (All on a Cr_2O_3 basis).

Alloy and Conditions	**Experimental Slope ($kg\ m^{-2}s^{-1}$)**	**Evaporation based on Glusko (14) $CrO_2(OH)_2(g)$ data ($kg\ m^{-2}s^{-1}$)**	**Evaporation based on Gindorf (18) $CrO_2(OH)_2(g)$ data ($kg\ m^{-2}s^{-1}$)**	**Evaporation based on Ebbinghaus (15) $CrO_2(OH)_2(g)$ data ($kg\ m^{-2}s^{-1}$)**
Haynes 230 UNS NO6230 760°C 38% H_2O in air 1.9×10^{-3} m s^{-1}	-3.46×10^{-10} (19)	-6.50×10^{-11}	-7.00×10^{-10}	-1.38×10^{-08}
Haynes 230 UNS NO6230 760°C 37% H_2O in air 7.6×10^{-3} m s^{-1}	-1.11×10^{-9} (19)	-1.27×10^{-10}	-1.37×10^{-9}	-2.69×10^{-08}
Inconel 625 NS NO6625 760°C 37% H_2O in air 1.9×10^{-3} m s^{-1}	-4.13×10^{-10}	-6.50×10^{-11}	-7.00×10^{-10}	-1.38×10^{-08}
304L UNS S30403 600°C 10% H_2O in O_2 2.5×10^{-2} m s^{-1}	-5.68×10^{-10} (4)	-3.79×10^{-11}	-5.23×10^{-10}	-1.03×10^{-08}

Since candidate alloys for this application are all chromia formers, reactive evaporation could be an important degradation mechanism. Representative environments for current and advanced steam turbines were chosen as: temperatures of 540, 600, 680, 720, 740, and 760°C, pressures of 16.5, 20.0, 31.0 and 34.5 MPa, steam velocity of 300 m s^{-1} (calculated from 60 Hz, 3600 revolutions per minute, and 0.8 m rotor + blade radius), and characteristic length of 0.05 m. This is turbulent flow, so Eq. 9 was used. The values used for the partial pressure of oxygen were based off of oxygenated feedwater that is typical of once-through supercritical power plants, *i.e.*, dissolved oxygen (DO) of 150-180 ppb and a pH of 8.0-8.5 controlled with ammonia additions (12). By the time

the feedwater enters the boiler, most of the DO has been removed to less than 1 ppb (20). However, at high temperatures, water undergoes dissociation to O_2 and H_2 to levels above 1 ppb. To estimate the DO at temperature and pressure, the program FactSage (21) was used to first determine the amount of NH_3 required for a pH of 8.25 at 25°C: 34.5 ppb. This agreed well with the reported (12) 20-65 ppb NH_3 used for pH control to 8.0 to 8.5. Next FactSage was used to find the value of P_{O2} for each temperature and pressure combination from water with 34.5 ppb NH_3. A minimum of 1 ppb of DO was used for cases where the dissociation pressure of O_2 was less than 1 ppb. Output from FactSage included the fugacities of H_2O and O_2, so these were used in place of PH_2O and PO_2 in Eq. 9. The use of fugacities made only a minor difference because the fugacity adjustments tended to cancel each other out in Eq. 9. Results are shown in Fig. 5 and Table 4.

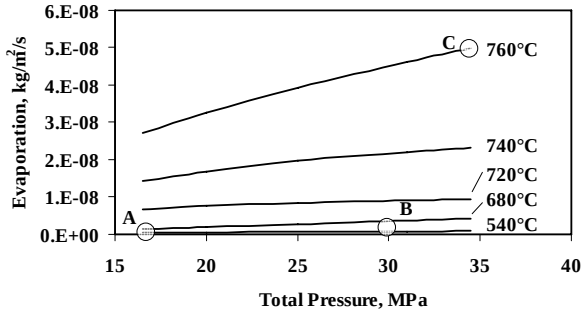

Figure 5. Predicted evaporation rates in supercritical steam turbine conditions with DO set by the greater of the dissociation of water or 1 ppb, 300 m s^{-1} flow rate, and a characteristic length of 0.05 m. Region "A" is typical for current power plants, "B" is for current advanced power plants, and "C" is the U.S. DOE target conditions.

These predicted rates are large compared to the experimental tests at atmospheric pressure and low gas velocities (Table 3). The highest value in Table 4 (for 760°C and 34.5 MPa) of 4.98×10^{-8} kg $m^{-2}s^{-1}$ is equivalent to 0.077 mm per year of solid Cr loss (assumes a metal density of 9 g cm^{-3} and a conversion to a Cr basis in a manner similar to Eq. 18). This is a large value for metal loss for a component expected to operate many years, and it may be larger if the scale losses enough Cr to become non-protective. Current state-of-the-art steam turbines operate at approximately 600°C and 31 MPa, with a predicted evaporation rate of 1.72×10^{-9} kg $m^{-2}s^{-1}$. Typical subcritical steam power plants operate at 538°C and 16.5 MPa, with a predicted evaporation rate of about 3.8×10^{-10} kg $m^{-2}s^{-1}$. These later two cases should have lower evaporation rates in practice because the ferritic-martensitic steels used usually form Fe-Cr spinel outer scales instead of chromia scales. This lowers the activity of chromia in the scale, which lowers the partial pressure of $CrO_2(OH)_2(g)$ (Eq. 16) and thus lower the evaporation rate.

Table 4 – Predicted Partial Pressures of $CrO_2(OH)_2$ and Evaporation Rates in Supercritical Steam Turbine Conditions with DO Set by the Greater of the Dissociation of Water or 1 ppb. There is also 34.5 ppb of NH_3.

T, °C	P_T, MPa	DO, ppb	O_2 fugacity coefficient	H_2O fugacity coefficient	$P_{CrO2(OH)2}$	k_e, kg m^{-2} s^{-1}
540	16.5	1	1.136	0.892	2.27E-12	3.85E-10
540	20.0	1	1.167	0.871	2.61E-12	5.03E-10
540	31.0	1	1.270	0.807	3.58E-12	8.28E-10
540	34.5	1	1.304	0.788	3.86E-12	9.58E-10
600	16.5	1	1.118	0.917	4.30E-12	7.35E-10
600	20.0	1	1.145	0.901	4.96E-12	9.54E-10
600	31.0	1	1.233	0.850	6.88E-12	1.72E-09
600	34.5	1	1.263	0.835	7.45E-12	2.00E-09
680	16.5	1	1.101	0.942	8.88E-12	1.49E-09
680	20.0	1	1.124	0.930	1.03E-11	1.94E-09
680	31.0	1	1.198	0.893	1.44E-11	3.68E-09
680	34.5	1	1.223	0.882	1.56E-11	4.30E-09
720	16.5	4.94	1.094	0.951	4.04E-11	6.71E-09
720	20.0	3.95	1.115	0.941	3.96E-11	7.58E-09
720	31.0	2.12	1.184	0.910	3.50E-11	9.14E-09
720	34.5	1.78	1.207	0.901	3.32E-11	9.35E-09
740	16.5	11.26	1.091	0.955	8.71E-11	1.43E-08
740	20.0	9.39	1.112	0.946	8.81E-11	1.68E-08
740	31.0	5.65	1.178	0.918	8.48E-11	2.21E-08
740	34.5	4.87	1.200	0.909	8.25E-11	2.31E-08
760	16.5	21.70	1.089	0.959	1.64E-10	2.72E-08
760	20.0	18.67	1.108	0.951	1.70E-10	3.25E-08
760	31.0	12.35	1.173	0.925	1.76E-10	4.62E-08
760	34.5	10.94	1.194	0.917	1.75E-10	4.98E-08

The presence of Cr evaporation taking place in the superheater tubes prior to the turbine may to some degree saturate the steam with $CrO_2(OH)_2(g)$, thereby reducing the driving force for evaporation. The lower steam velocity in the superheater tubes (10-25 m s^{-1} is typical (12)) will result in lower evaporation rates than in the steam turbine (~300 m s^{-1}), but there is considerable length of superheater tubing at the high temperature and pressure of the high pressure turbine that could allow some build up of $CrO_2(OH)_2(g)$. Evaporation in the superheater may move the problem upstream and reduce it in the turbine.

Laboratory Experimentation

Laboratory corrosion tests generally seek to mimic the process environment as closely as possible. In cases where this is difficult, then one seeks to establish conditions where the corrosion mechanisms are the same. For steam turbines, laboratory tests with the same combination of temperature, pressure, gas velocities, and steam chemistry are extremely difficult and expensive. Therefore tests sacrifice one or more of the conditions—usually pressure or gas velocity.

For examining the effects of Cr-evaporation as a corrosion mechanism, laboratory tests may be best served with much higher oxygen partial pressures so as to increase the evaporation rate. A comparison of the evaporation rates from Tables 3 and 4 show that even with air and water vapor mixtures, experimental tests (Table 3) fail to achieve the predicted evaporation rates at high pressures and gas flows (Table 4) by several orders of magnitude. As discussed earlier, for O_2+H_2O mixtures, a P_{H2O} equal to $4/7P_{O2}$ (~57% H_2O) should maximize the evaporation rate. The same holds true (albeit at a lower evaporation rate) for air+H_2O mixtures with the maximum also at 57% H_2O. Laboratory tests in steam at atmospheric pressure will have extremely small evaporation rates due to the low partial pressure of oxygen. This is all illustrated in Fig. 6 for predictions made at 760°C. In Fig. 6 the advanced steam turbine points are from the 760°C data in Table 4. The representative laboratory curves are a function of the partial pressure of O_2 in either air+H_2O or O_2+H_2O atmospheres. The laboratory curves were all calculated at atmospheric pressure, a relatively large laboratory gas velocity of v = 0.02 m s^{-1}, and L = 0.02 m. The right-hand-side of the laboratory curves drop sharply as P_{H2O} approaches zero. The right-hand-side of the laboratory curves are limits. Reactive evaporation in drier O_2 or drier air would switch at that point from $CrO_2(OH)_2(g)$ being the dominate gas specie to $CrO_3(g)$, and would not drop further with less H_2O.

Efforts to improve laboratory tests for higher evaporation rates would include testing in either O_2+H_2O or Air+H_2O at 57% H_2O, increasing the gas velocity (k_e is proportional to $v^{½}$), increasing the sample size (k_e is proportional to $L^{½}$), or increasing the total pressure (moving the reaction of Eq. 2 to the right).

Conclusions

A methodology was developed to calculate Cr evaporation rates from Cr_2O_3 with a flat planar geometry. As part of this calculation, the interdiffusion coefficient, absolute viscosity, and the Gibbs energy of reaction were determined. The major variables include temperature, total pressure, gas velocity, and gas composition. Experimental verification was done at atmospheric pressure in moist air and moist oxygen. It was concluded that the Gindorf *et al.* (18) data for $\Delta G_{f,\ CrO2(OH)2}$ gave a close match with observed evaporation rates, and so was used for further calculations.

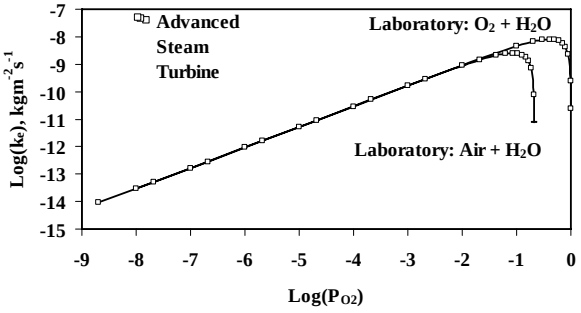

Figure 6. Predicted evaporation rates at 760°C for advanced steam turbines (DO set by dissociation, P_T of 25.0, 31.0, and 34.5 MPa, v = 300 m/s, L = 0.05 m) compared with atmospheric pressure laboratory tests (v = 0.02 m/s, L = 0.02 m) as a function of the partial pressure of O_2 for tests in either O_2+H_2O or Air+H_2O.

The methodology was also applied to advanced steam turbines conditions. The high velocities and pressures of the advanced steam turbine led to evaporation predictions as high as 4.98×10^{-8} kg $m^{-2}s^{-1}$ at 760°C and 34.5 MPa. This is equivalent to 0.077 mm per year of solid Cr loss. Should this Cr loss be too large to maintain sufficient Cr for a protective oxide scale, then much higher oxidation rates could result. Chromium evaporation is expected to be an important oxidation mechanism with the types of nickel-base alloys proposed for use above 650°C in advanced steam boilers and turbines. Chromium evaporation is of less importance for the ferritic and austenitic alloys used in current steam boilers and turbines due to their relatively large oxidation rates with respect to evaporation rates.

It was shown that laboratory experiments, with much lower steam velocities and usually much lower total pressure than found in advanced steam turbines, would best reproduce chromium evaporation behavior with atmospheres that approach either O_2+H_2O or Air+H_2O at 57% H_2O instead of with oxygenated steam.

References

1. Robert Swanekamp, "Return of the Supercritical Boiler," *Power*, 146 (4), 2002, pp. 32-40.

2. R. Viswanathan, J. F. Henry, J. Tanzosh, G. Stanko, J. Shingledecker, B. Vitalis, R. Purgert, "U.S. Program on Materials Technology for Ultra-Supercritical Coal Power Plants," *Journal of Materials Engineering and Performance*, 14, 2005, pp. 281-292.

3. H. Asteman, J.-E. Svensson, L.-G. Johansson, M. Norell, "Indication of Chromium Oxide Hydroxide Evaporation During Oxidation of 304L at 873 K in the Presence of 10% Water Vapor," *Oxidation of Metals*, 52, 1999, pp. 95-111.

4. H. Asteman, J.-E. Svensson, M. Norell, L.-G. Johansson, "Influence of Water Vapor and Flow Rate on the High-Temperature Oxidation of 304L; Effect of Chromium Oxide Hydroxide Evaporation," *Oxidation of Metals*, 54, 2000, pp. 11-26.

5. David R. Gaskell, *An Introduction to Transport Phenomena in Materials Engineering*, New York, New York: Macmillan Publishing, 1992, pp. 78-89, 569-578.

6. G. H. Geiger, D. R. Poirier, *Transport Phenomena in Metallurgy*, Reading, Massachusetts: Addison-Wesley Publishing, 1973, pp. 7-13, 463-467, 529-537.

7. William A. Tucker, Leslie H. Nelken, "Diffusion Coefficients in Air and Water," in *Handbook of Chemical Property Estimation Methods*, Eds. Warren J. Lyman, William F. Reehl, David H. Rosenblatt Washington DC: American Chemical Society, 1990, pp. 17.1-17.25.

8. Edward N. Fuller, Paul D. Schettler, J. Calvin Giddings, "A New Method for Prediction of Binary Gas-Phase Diffusion Coefficients," *Industrial & Engineering Chemistry*, 58, 1966, pp. 19-27.

9. S. Veliah, K.-H. Xiang, R. Pandey, J. M. Recio, J. M. Newsam, "Density Functional Study of Chromium Oxide Clusters: Structures, Bonding, Vibrations and Stability," *Journal of Physical Chemistry B*, 102, 1988, pp. 1126-1135.

10. R. Byron Bird, Warren E. Stewart, Edwin D. Lightfoot, *Transport Phenomena*, New York, New York: John Wiley & Sons, 1960, pp. 504-506.

11. J. C. Slattery, R. B. Bird, "Calculation of the Diffusion Coefficient of Dilute Gases and of the Self-Diffusion Coefficient of Dense Gases, "American Institute of Chemical Engineers Journal, 4, 1958, pp. 137-142.

12. *Steam*, 40th ed., Eds. S. C. Stultz, J. B. Kitto, Barberton, Ohio: Babcock & Wilcox, 1992, pp. 3.8-3.9, 42.11.

13. Elizabeth J. Opila, "Volatility of Common Protective Oxides in High-Temperature Water Vapor: Current Understanding and Unanswered Questions," *Materials Science Forum*, 461-464, 2004, pp. 765-774.

14. Glusko Thermocenter of the Russian Academy of Sciences—Izhorskaya 13/19, 127412, Moscow, Russia: IVTAN Association, 1994.

15. B. B. Ebbinghaus, "Thermodynamics of Gas Phase Chromium Species: The Chromium Chlorides, Oxychlorides, Fluorides, Oxyfluorides, Hydroxides, Oxyhydroxides, Mixed Oxyfluorochlorohydroxides, and Volatility Calculations in Waste Incineration Processes, *Combustion and Flame*, 93, 1993, pp. 119-137.

16. V. S. Yungman, V. A. Medvedev, I. V. Veits, G. A. Bergman, IVTANTHERMO—A Thermodynamic Database and Software System for the Computer, Boca Raton, Florida: CRC Press and Begell House, 1993.

17. A. Roine, HSC Chemistry 5.11, Pori, Finland: Outokumpu Research Oy, 2002.

18. C. Gindorf, K. Hilpert. L. Singheiser, "Determination of Chromium Vaporization Rates of Different Interconnect Alloys by Transpiration Experiments, *Solid Oxide Fuel Cells (SOFC VII)*, Eds. H. Yokokawa, S. C. Singhal, Proceedings Vol. 2001-16, Pennington, New Jersey: Electrochemical Society, 2001, pp. 793-802.

19. G. R. Holcomb, M. Ziomek-Moroz, D. E. Alman, "Oxidation of Alloys for Advanced Steam Turbines," *Proceedings of the 23rd Annual Pittsburgh Coal Conference*, Pittsburg, Pennsylvania: University of Pittsburg, 2006.

20. Steven C. Kung, The Babcock & Wilcox Company, Private Communication, June 2007.

21. C. W. Bale, A. D. Pelton, W. T. Thompson, G. Eriksson, K. Hack, P. Chartrand, S. Decterov, J. Melançon, S. Petersen, FactSage 5.5, Thermfact and GTT-Technologies, 1976-2007.